Bremsstrahlung photons from the bare surface of a strange quark star

Prashanth Jaikumar*[1], Charles Gale[1], Dany Page[2], and Madappa Prakash[3]
[1] *Physics Department, McGill University, Montréal, Québec H3A 2T8, Canada.*
[2] *Instituto di Astronomia, UNAM, Mexico D.F. 04510, Mexico.*
[3] *Department of Physics & Astronomy, SUNY at Stony Brook, Stony Brook, NY 11794, USA.*

The photon emissivity from the bremsstrahlung process $e^-e^- \to e^-e^-\gamma$ occuring in the electrosphere at the bare surface of a strange quark star is calculated. For surface temperatures $T < 10^9$K, the photon flux exceeds that of e^+e^- pairs that are produced via the Schwinger mechanism in the presence of a strong electric field that binds electrons to the surface of the quark star. The average energy of photons emitted from the bremsstrahlung process can be 0.5 MeV or more, which is larger than that in e^+e^- pair annihilation. The observation of this distinctive photon spectrum would constitute an unmistakable signature of a strange quark star and shed light on color superconductivity at stellar densities.

PACS: 26.60.+c, 95.30.Cq, 97.60.Jd

I. INTRODUCTION

Recently, it has been pointed out that thermal emission from the bare surface of a strange quark star, due to both photons and e^+e^- pair production, can produce luminosities well above the Eddington limit ($\sim 10^{38}$ erg sec^{-1}) for extended periods of time, from about a day to decades, depending on the superconducting phase of quark matter [1]. The spectrum of emitted photons is significantly different from that of a normal cooling neutron star ($30 < E/\text{keV} < 500$ instead of $0.1 < E/\text{keV} < 2.5$). This distinctive spectrum and temperature evolution, if observed, would constitute an unmistakable detection of a strange quark star and shed light on color superconductivity at stellar densities. The predicted characteristics are well within the capabilities of the INTEGRAL satellite [2] launched toward the end of 2002.

A strange quark matter (SQM) star differs from a normal neutron star (NS) in several important ways, which include

(1) A SQM star is self-bound [3–7] while a NS requires gravitational forces for its binding. As a consequence, the pressure vanishes at vanishing baryon density in a NS with a surface of normal matter. The interior of the NS, however, may contain any or a combination of non-nucleonic matter such as hyperons, pion or kaon condensates, or quark matter [8,9]. In contrast, a self-bound SQM star is made entirely of quark matter up to its bare surface and the pressure vanishes at a finite but supra-nuclear baryon density. In the context of the MIT bag model with first order corrections due to gluon exchange, the baryon density n_B at which the pressure vanishes is [10]

$$n_B(P=0) = \left(\frac{4B}{3\pi^{2/3}}\right)^{3/4}\left(1-\frac{2\alpha_c}{\pi}\right)^{1/4}, \tag{1}$$

where B is the bag constant and $\alpha_c = g_c^2/(4\pi)$ is the quark-gluon coupling constant. For typical values of B and α_c [5], the baryon density at vanishing pressure is about 2 to $3n_0$, where $n_0 = 0.16$ fm^{-3} is the saturation density of nuclear matter. The density in Eq. (1) is not significantly affected by the finite strange quark mass [10] or by pairing gaps in the quark phase [11].

(2) The mass versus radius relations of NS and SQM stars differ significantly, although in the range of masses ($1 < M/M_\odot < 2$) observed to date [12], the calculated radii are similar ($R \sim 10$ to 15 km). This makes it difficult to distinguish these two classes on the basis of their gross physical properties alone.

The light curves of NS and SQM stars, determined by surface photon emission, can however be very different under certain conditions. Central to the discussion of photon emission from a SQM star is the physical size and composition of its surface layer. If quark matter is in the Color-Flavor-Locked (CFL) superconducting phase (in which all three flavors take part in pairing) up to the surface, no electrons are required or admitted [13–15]. Surface photon emission from the CFL phase has been found to saturate the blackbody limit at early times [16]. In contrast, charge neutrality cannot be satisfied by three flavors of quarks alone in the two-flavor superconducting phase (2SC). In this case, an electron concentration n_e/n_B of about 10^{-4} to 10^{-3} is required to achieve

*jaikumar@hep.physics.mcgill.ca

charge neutrality. Normally, the bare surface of a quark star is an inefficient emitter of thermal radiation below temperatures $T \sim 10^{11}$K because the plasma frequency of quark matter is high, of order 20 MeV [17]. However, in the 2SC phase, strong electric fields can arise because electrons in the surface layer are bound by electrostatic interaction to quark matter. This layer of electrons, which we will call the "electrosphere", is typically 10^3 fm thick [17] and can have radial electric fields whose magnitude ($\sim 5 \times 10^{17}$ V cm^{-1}) exceeds the critical value required for electron-positron pair production from the QED vacuum. The critical value for the electric field was estimated by Schwinger to be [18]

$$E_{\rm cr} = \frac{m_e^2 c^3}{e\hbar} \simeq 1.3 \times 10^{16} \text{ V cm}^{-1} \quad , \tag{2}$$

where m_e and e are the electron's mass and charge, respectively. For a homogeneous electric field $E \gg E_{\rm cr}$, the vacuum pair-creation rate per unit volume is given by [18]

$$R_{\pm} = \frac{m_e^4 c^5}{24\pi\hbar^4}\left(\frac{E}{E_{\rm cr}}\right)^2 \simeq 1.7 \times 10^{50}\left(\frac{E}{E_{\rm cr}}\right)^2 \text{ cm}^{-3} \text{ s}^{-1} \, . \tag{3}$$

Usov [19] first exploited the possibility of thermal emission of hard photons from the annihilation of e^+e^- pairs created by super-critical electric fields in degenerate matter and demonstrated that the associated photon emissivity is large enough to be observable. Subsequently, Page and Usov [1] have shown that the bare surface of a quark star under super-critical electric fields leads to a light curve that is significantly different from those produced by either quark matter surrounded by a layer of normal matter, or by surfaces of compact objects made entirely of normal matter. Their principal conclusion was that hard photon emission from e^+e^- annihilation can dominate significantly over the blackbody spectrum at lower luminosities, and that the variation in the photon spectrum with luminosity could be used as an observational signature of a young bare strange quark star. Furthermore, calculations of light curves from quark matter in its superconducting phases (CFL or 2SC) have shown that it may be possible to set bounds on quark pairing gaps provided they are in the range 0.5 MeV to a few MeV [1].

Our objectives in this paper are to
(1) point out that, depending on the temperature, the bremsstrahlung process $e^-e^- \to e^-e^-\gamma$ in the electrosphere can lead to photon luminosities that are significantly larger than the e^+e^- pair production luminosities in the presence of strong electric fields,
(2) present a calculation of the corresponding emissivity including minimal screening effects, and investigate the role of the Landau-Pomeranchuk-Migdal (LPM) effect, and
(3) compare the photon emissivity from the $e^-e^- \to e^-e^-\gamma$ bremsstrahlung process to other processes occurring in the thin electrosphere at the surface of the star. Examples of such processes include e^+e^- pair production which occurs due to the presence of strong electric fields, and equilibrium and non-thermal bremsstrahlung radiation from quark-quark collisions in the uppermost layer of quark matter.

We wish to emphasize that our discussion applies only to the case in which a charge neutralizing surface electron layer is present. This can be realized in the 2SC, the gapless CFL (gCFL) or crystalline color superconducting phases [14,20], but not in the pure CFL phase.

This paper is organized as follows. Sec. II is devoted to a qualitative discussion of photon propagation in the electrosphere. Here the physical characteristics of the electrosphere, the photon mean free path, the photon dispersion relation, and the role of the Landau-Pomeranchuk-Migdal (LPM) effect that suppresses the emission of low-energy photons are addressed. The calculation of the photon emissivity from the bremsstrahlung process in degenerate matter (with and without modifications from the LPM effect) in the electrosphere, and a characterization of the non-thermal nature of the emitted photon spectrum are detailed in Sec. III. This section also contains numerical results and discussion of the bremsstrahlung radiation flux, including a comparison with the flux of the e^+e^- pair annihilation process and quark-related processes. Sec. IV contains our conclusions and outlook. Appendix A outlines the evaluation of an integral required in Sec. III.

II. PHOTON PROPAGATION IN THE ELECTROSPHERE

At the surface of the bare quark star, the density of quarks drops abruptly to zero within a layer of thickness of about 1 fm, this length scale being set by the range of the strong interaction. The density profile of the electrons can be determined by solving the Poisson equation in the Thomas-Fermi approximation. In the plane-parallel approximation for the layer of the electrosphere, the electron chemical potential as a function of distance z from the quark surface is given by [21]

$$\mu_e(z) = \frac{\mu_e(0)}{1 + z/H}; \quad H = \frac{\hbar\, c}{\mu_e(0)}\sqrt{\frac{3\pi}{2\alpha}} = 501.3\left(\frac{10 \text{ MeV}}{\mu_e(0)}\right) \text{ fm}\,, \tag{4}$$

where $\alpha = e^2/4\pi$ is the fine structure constant. For a typical $\mu_e(0) = (10 - 20)$ MeV, the electrosphere is about 10^3 fm thick or more. The variation of μ_e across the electrosphere is shown in Fig. 1. The number density of electrons at the surface of such a star is $n_e \sim 3 \times (10^{-5} - 10^{-4})$ fm^{-3} [17]. The electron degeneracy parameter $\lambda = n_e^{1/3} h/\sqrt{m_e T} \gg 1$ for temperatures below 10^{10} to 10^{11}K ($\sim (1 - 10)$ MeV), which is the case some tens of seconds after the star is born. Thereafter, electrons quickly settle into a degenerate Fermi sea, and their Fermi momentum far exceeds their rest mass, making it a relativistic degenerate system.

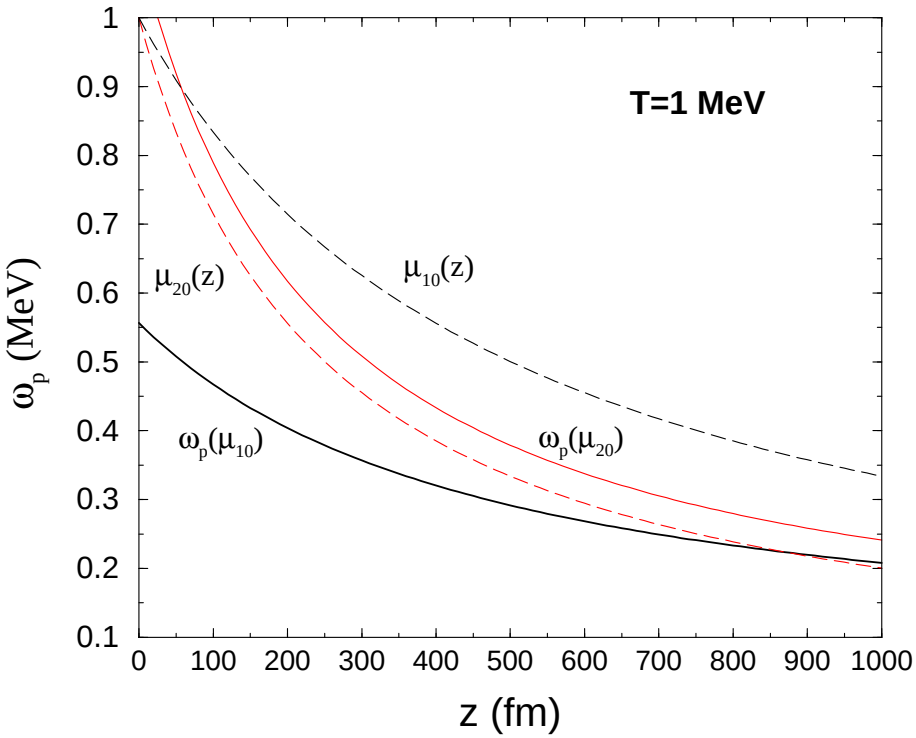

FIG. 1. Profiles of the electron chemical potential μ_e (Eq. (4)) and the plasma frequency ω_p in the degenerate limit (Eq. (6)) versus distance z from the surface of the strange quark matter star. μ_{10} (μ_{20}) is the electron chemical potential in units of 10 (20) MeV.

The optical depth of the electron layer is determined by the mean number of scatterings of photons on electrons. Bremsstrahlung photons from this layer would mostly have energies much smaller than the Fermi energy ($\epsilon_F = k_B T_F$) of the electrons. Since electrons can only manoeuvre within an energy window $\Delta\epsilon \sim \frac{\pi^2}{12}\epsilon_F \left(\frac{T}{T_F}\right)^2$ in a typical scattering process, and $T \ll T_F$ due to strong degeneracy, the typical energy of the emitted photons would be of order $\Delta\epsilon$. The electron in the intermediate state remains almost on-shell.

The ratio of the photon energy to electron mass is the small parameter that justifies an estimate of the photon mean free path based on the Thomson cross-section. If this ratio is of order unity or larger, the Compton cross-section should be used. For a given electron density, the photon mean free path is

$$l_T \simeq \frac{1}{n_{eff}\sigma_T}, \quad \sigma_T = \frac{8\pi\alpha^2}{3m_e^2} = 66.54 \text{ fm}^2 \quad , \tag{5}$$

where σ_T is the Thomson cross section. The quantity $n_{eff} \approx n_e(T = 0)(T/\mu_e)$ is the effective number density of electrons, which takes into account the fact that in a degenerate gas the available scattering states are restricted to the vicinity of the Fermi surface. For an electron density of $n_e = 3.53 \times 10^{-5}$ fm^{-3} (corresponding to a chemical potential of $\mu_e = 20$ MeV), and $T = 10^{11}$K (8.6 MeV), this yields a mean free path ~ 1000 fm. For higher photon energies, the mean free path using the Compton cross-section is somewhat larger. The electron layer, being about a 1000 fm thick, is therefore transparent to photons.

Since the emitted photons do not scatter often enough to become thermalized, the electrosphere is a source of non-thermal low energy photons. We will quantify this non-thermal nature by calculating the ratio of the second to first moment of the photon energy spectrum and comparing it with a similar ratio (a fixed $T-$ independent number) for the Planckian spectrum.

To a very good approximation, the dispersion relation of the emitted electromagnetic wave in the plasma can be taken as $\omega = (\omega_p^2 + k^2)^{1/2}$ (in $c = 1$ units). The plasma frequency ω_p serves as a low-energy cut-off. For degenerate electrons ($T/\mu_e \ll 1$), the plasma frequency is determined from [22]

$$\omega_p^2 \cong \frac{4\alpha}{3\pi}\mu_e^2\left(1 + \frac{\pi^2 T^2}{3\mu_e^2}\right). \tag{6}$$

Only photons with $\omega > \omega_p$ can propagate without severe attenuation by the plasma. The plasma frequency, being density-dependent, decreases with increasing z (Fig. 1). This implies that photons emitted toward the surface from the lower layers of the electrosphere can escape. A large plasma frequency, however, implies an overall suppression of the emissivity. The optical depth of the electrosphere at any distance is determined by the plasma frequency, which in turn is a function of the electron density profile. The emissivity Q is thus a function of $\omega_p(z)$. The total luminosity can be expressed as

$$L = 4\pi R_s^2 \int_{z=0}^{z=z_0} Q(\omega_p(z))\, dz\,, \tag{7}$$

where z_0 is the thickness of the electrosphere, and R_s the radius of the star.

It should be noted that some (possibly paired) quark matter is admixed with electrons in the innermost region (of thickness about 1 fm) of the electrosphere. The screening effect of quark or electron matter will be taken into account in our calculation by modifying appropriately the exchanged photon that mediates the e^-e^- scattering. We will see that electric screening and magnetic damping effects play only a small role for emission of low energy photons. Such photons can escape despite the large plasma frequency ω_p (~ 20 MeV) of the ambient quark matter because the thickness of the electron layer is about the same as $c/\omega_p \sim 10^{-12}$ cm.

Bremsstrahlung radiation is known to be suppressed by multiple scattering of electrons (LPM effect [23]) within the formation time of the emitted photon. This is especially relevant for low energy photons (which have a large formation time) that are emitted mostly in the forward direction (small emission angles). The LPM effect is important for wave numbers $k \le k_c$ that satisfy [24]

$$k_c = \frac{E_e^2}{E_{LPM}}\,, \tag{8}$$

where E_e is the typical energy of the emitting particle. For degenerate electrons of energy $\mu_e \sim (10 - 20)$ MeV, the quantity E_{LPM} is given by [25]

$$E_{LPM}(\mathrm{eV}) = 3.8 \times 10^{12} X_0(\mathrm{cm})\,. \tag{9}$$

Above, X_0 is the typical radiation length in the medium. If, for simplicity, we assume a static screened Coulomb interaction between electrons, the radiation length is energy independent for high energies of the emitting particles, and is given by [1]

$$X_0 = \frac{m_e^2}{4 n_e \alpha^3 \ln(183)}\,, \tag{10}$$

which yields $E_{LPM} = 70$ keV and $k_c \sim 1.4$ GeV for $\mu_e = 10$ MeV. This large value of E_{LPM} implies that the LPM effect will strongly suppress the number of photons radiated. For a photon of wave number k, the factor by which the bremsstrahlung process is reduced is given by [24]

$$S_{LPM}(k) = \sqrt{\frac{k E_{LPM}}{E_e^2}} \simeq \frac{1}{300}\,, \tag{11}$$

where in quoting the numerical result above, we have used $\mu_e = 10$ MeV and $k = 0.5$ MeV as an example. This reduction shows that the inclusion of the LPM effect is important for a realistic estimate of the emissivity. The LPM suppression depends on the density of scatterers through μ_e.

---

[1] Although we use the zero-temperature expression for n_e here, the available scattering states are properly accounted for by the Fermi functions in the LPM calculation to follow.

III. PHOTON EMISSIVITY FROM THE BREMSSTRAHLUNG PROCESS

The photon emissivity from the bremsstrahlung process is

$$Q = \frac{2\pi}{s\hbar} \quad \left[\prod_{i=1}^{4}\int \frac{d^3p_i}{(2\pi)^3 2\omega_{p_i}}\right]\int \frac{d^3k}{(2\pi)^3 2\omega_k}\omega_k \sum_{spin}|M|^2\ S_{LPM}(k) \tag{12}$$
$$\times\, n_F(\omega_{p_1})n_F(\omega_{p_2})\tilde{n}_F(\omega_{p_3})\tilde{n}_F(\omega_{p_4})(2\pi)^3\delta^3(\mathbf{P_f}-\mathbf{P_i})\delta(E_f-E_i) \quad .$$

The subscripts $i = 1$ to 4 refer to electrons (1,2 label the incoming states and 3,4 the outgoing states), whereas $(\omega_k, \mathbf{k})$ refer to the 4-momentum of the emitted photon. The symmetry factor $s = 2$. The phase space for electrons is convoluted with the appropriate Fermi distribution functions $n_F(\omega_{p_i}) = 1/(\mathrm{e}^{\omega_{p_i}/T}+1)$ (in $k_B = 1$ units) and $\tilde{n}_F = 1-n_F$, respectively. For simplicity, and to highlight the role of the LPM effect, we first obtain the analytic T and μ_e dependences of the emissivity without the LPM suppression factor. The effects of the LPM effect are investigated in the second stage. In this case, an analytical analysis becomes unwieldy and hence we present results of numerical calculations. A comparison of the respective emissivities enables an overall assessment of the importance of in-medium multiple scattering effects.

A. The Bremsstrahlung Process in Degenerate Matter

For conditions of interest here, electrons in the electrosphere are strongly degenerate. The emissivity will thus be dominated by low energy photons ($\omega_p < \omega_k \ll \mu_e$). The contribution from high energy photons ($\omega_k \gg m_e$), which requires a full quantum calculation of the bremsstrahlung process, is expected to be small. We utilize the quasiclassical approximation for low energy photons, in which case the calculation of the emissivity simplifies if we use Low's theorem for bremsstrahlung [26].

Low's theorem states that the first two terms in the differential cross-section of bremsstrahlung, expressed as a power series in the energy loss ω_k, is unique and exactly calculable in terms of the corresponding elastic amplitude. The presence of the factor ω_k in the numerator of Eq. (12) ensures that in the low energy limit, the dominant contribution to Q is non-singular and can be estimated once the leading term in the series ($\sim 1/\omega_k$) is established. Retaining only the first term in Low's soft-photon expansion shows that the full scattering amplitude for bremsstrahlung factorizes into an elastic part, which is Møller scattering, and a part which gives the classical intensity of photon emission divided by the energy ω_k. At low energy, the probability of successive photon emission is enhanced, which causes a naive perturbative expansion in powers of the electromagnetic coupling to fail. The differential cross-section can alternatively be understood in terms of the mean number of photons emitted, which is equivalent to the classical intensity divided by the mean energy of one photon. This factorization of amplitudes simplifies our calculation to a large extent. The energy exchange in e^-e^- scattering being small, we can write the matrix element explicitly as

$$iM = M_{el}\left[e\left(\frac{p_4.\epsilon^*}{p_4.k} - \frac{p_2.\epsilon^*}{p_2.k} + \frac{p_3.\epsilon^*}{p_3.k} - \frac{p_1.\epsilon^*}{p_1.k}\right)\right] \quad , \tag{13}$$

where M_{el} denotes the interaction for elastic scattering of the incoming electrons, ϵ^μ denotes the polarization vector of the photon, and e is the charge of the electron. The term in the second bracket in Eq. (13) is the familiar result from classical radiation theory for an electron that accelerates under an impulsive force. In the low-energy limit, the emission from the exchange diagrams simply doubles the overall result for the emissivity from the direct diagrams (no interference). Since there is a symmetry factor of $s = 2$ in the denominator of the emissivity expression Eq. (12), we may ignore the identity of the particles altogether and evaluate the emissivity from the direct diagrams alone. The spin sum can be performed separately over the electrons and the photon thanks to the decoupling at low energy. We are thus led to the following expression for the emissivity

$$Q = \frac{1}{\hbar}\int \frac{d^3p_1}{(2\pi)^3}\frac{d^3p_2}{(2\pi)^3}n_F(\omega_{p_1})n_F(\omega_{p_2})\int d\omega_k\,\omega_k\left(\frac{d\sigma}{d\omega_k}\right) \quad ; \tag{14}$$

$$\left(\frac{d\sigma}{d\omega_k}\right) = (d\sigma_{el})\frac{\sqrt{\omega_k^2-\omega_p^2}}{2}\int\frac{d\Omega_k}{(2\pi)^3}\sum_{\lambda=1,2}e^2\left|\frac{p_4.\epsilon^*_\lambda}{p_4.k} - \frac{p_2.\epsilon^*_\lambda}{p_2.k} + \frac{p_3.\epsilon^*}{p_3.k} - \frac{p_1.\epsilon^*}{p_1.k}\right|^2 \quad , \tag{15}$$

$$(d\sigma_{el}) = \frac{1}{2\omega_{p_1}}\frac{1}{2\omega_{p_2}}\left(\prod_{f=3,4}\frac{d^3p_f}{2\omega_{p_f}}\right)\sum_{s=\pm}|M_{el}|^2(2\pi)^3\delta^3(\mathbf{P_f}-\mathbf{P_i})2\pi\delta(E_f-E_i)\tilde{n}_F(\omega_{p_3})\tilde{n}_F(\omega_{p_4}) \quad .$$

The change of variable from k to ω_k introduces the square root factor as the Jacobian, and the integration over ω_k runs from ω_p to ∞. Medium modifications to bremsstrahlung emission can be encapsulated in the refractive index of the electron plasma $n = \sqrt{1-\omega_p^2/\omega_k^2}$. With the definitions $\mathbf{p} = E\mathbf{v}$ and $\mathbf{k} = \omega_k\mathbf{n} = \omega_k n\hat{\mathbf{n}}$, where $|\hat{\mathbf{n}}| = 1$, the angular integral in Eq. (15) is

$$\int \frac{d\Omega_k}{(2\pi)^3} \sum_{\lambda=1,2} \frac{e^2}{\omega_k^2} \left[\left(\frac{p_4 \cdot \epsilon^*}{E_4 \tilde{n}_- \left[1 - \frac{n}{\tilde{n}_-} \mathbf{v}_4 \cdot \hat{\mathbf{n}} \right]} - \frac{p_2 \cdot \epsilon^*}{E_2 \tilde{n}_+ \left[1 - \frac{n}{\tilde{n}_+} \mathbf{v}_2 \cdot \hat{\mathbf{n}} \right]} + \frac{p_3 \cdot \epsilon^*}{E_3 \tilde{n}_- \left[1 - \frac{n}{\tilde{n}_-} \mathbf{v}_3 \cdot \hat{\mathbf{n}} \right]} - \frac{p_1 \cdot \epsilon^*}{E_1 \tilde{n}_+ \left[1 - \frac{n}{\tilde{n}_+} \mathbf{v}_1 \cdot \hat{\mathbf{n}} \right]} \right) \right]^2 \tag{16}$$

where $\tilde{n}_\pm \equiv 1 \pm \frac{1}{2} \frac{\omega_p^2}{E\omega_k}$ and we have neglected terms like $\gamma \cdot \epsilon^* \, \gamma \cdot k$ in the numerators compared to $\epsilon^* \cdot p$. Since $\omega_k \simeq \omega_p \ll E \simeq \mu_e$, we may approximate $\hat{n}_+ = \hat{n}_- = 1$. Although the refractive index $n \ll 1$, we cannot neglect the factors $[1 - \mathbf{v}_i \cdot \hat{\mathbf{n}}]$ in the denominator, since that would make the matrix element vanish by momentum conservation ($\sum_i v_i = 0$). Thus, for small n, the leading contribution to the squared matrix element for bremsstrahlung is $\mathcal{O}(n^2)$ and to the cross section $\mathcal{O}(n^3)$, one power of n coming from the Jacobian in Eq. (15). This allows us to perform an expansion of the angular integral in even powers of n. To $\mathcal{O}(n^2)$, and in the ultra-relativistic limit, the angular integral over $d\Omega_k$ can be evaluated, and one finds

$$\left(\frac{d\sigma}{d\omega_k} \right) = (d\sigma_{el}) \left[\frac{8\alpha}{5\pi} \frac{n^3 \sin^2 \theta_{CM}}{\omega_k} \right], \tag{17}$$

where $\alpha = e^2/(4\pi)$ is the fine structure constant and θ_{CM} is the angle in the centre of mass (henceforth CM) frame. In comparison, the vacuum result is [27]

$$\left(\frac{d\sigma}{d\omega_k} \right) = (d\sigma_{el}) \left[\alpha \frac{F(\xi)}{\omega_k} \right], \tag{18}$$

with

$$F(\xi) = \frac{2}{\pi} \left[\frac{2\xi^2 + 1}{\xi \sqrt{\xi^2 + 1}} \ln(\xi + \sqrt{(\xi^2 + 1)}) - 1 \right]; \qquad \xi = \frac{E}{m_e} \sin\left(\frac{\theta_{CM}}{2} \right) \quad .$$

The function $F(\xi)$ reduces to $8\xi^2/3\pi$ in the limit $\xi \ll 1$ (small angle scattering in the CM frame) which is the region of interest here. A comparison of the vacuum and medium expressions reveals a suppression factor of order $n^3 \times (m_e/\mu_e)^2$ due to the refractive index n of the medium.

In general, there are two conditions that must be satisfied for the validity of the two preceding equations. The first is that $m_e/E \ll 1$, because electromagnetic radiation from fast-moving particles is emitted roughly in a very narrow cone of this opening angle (this is equivalent to $\xi \ll 1$). Secondly, the exchanged photon 3-momentum $\mathbf{q}$ should be much larger than the change in $\mathbf{q}$ induced by soft photon emission [27]. Explicitly,

$$\left(\frac{\omega_k m_e^2}{E^3} \right) \ll \theta_{CM} \ll \left(\frac{m_e}{E} \right) \tag{19}$$

in the ultra-relativistic case. These limits on θ_{CM} suffice to give results for $d\sigma/d\omega_k$ that are correct to logarithmic accuracy. To be more accurate, one needs to go beyond the quasi-classical approximation which is not required for our purposes, since we are only interested in the emission of low energy photons. Emission of photons with large energies is severely supressed by Pauli blocking in the degenerate electron sea, and makes a negligible contribution to the emissivity.

The soft photon limit also simplifies the calculation of the in-medium elastic scattering cross section ($d\sigma_{el}$). The scattering occurs via the exchange of a screened photon propagator. Based on the general principle of gauge invariance, we can use Weldon's decomposition [28] of the amplitude

$$M_{el} = J_\mu(p_1, p_3) D^{\mu\nu}(q_0, \mathbf{q}) J_\nu(p_2, p_4); \quad J_\mu(p_i^{in}, p_j^{out}) = e\bar{u}(p_j)\gamma_\mu u(p_i) \quad , \tag{20}$$

and write it in terms of the transverse and longitudinal (temporal) parts of the one-loop self-energy as

$$M_{el} = J_\mu D^{\mu\nu}(q) J_\nu = \frac{J_0 J_0}{\mathbf{q}^2 + \Pi_L} + \frac{J_t J_t}{q^2 - \Pi_T} \quad , \tag{21}$$

where the exchange 4-momentum $q = (q_0, \mathbf{q}) = p_1 - p_3 = p_4 - p_2$. Heiselberg and Pethick [29] have shown that in the limit of small $q_0, |\mathbf{q}| \ll E \sim \mu_e$, the magnetic part of the electron current (spin flips) can be neglected, as is evident from Gordon's identity [30]. In this case, the electron current reduces to $J_\mu(p_i^{in}, p_j^{out}) \to 2e p_{i_\mu}^{in}$. The squared matrix element then becomes

$$|M_{el}|^2 = 16 \; e^4 E_1^2 E_2^2 \left| \frac{1}{\mathbf{q}^2 + \Pi_L} + \frac{(1 - x^2)\cos\phi}{q^2 - \Pi_T} \right|^2 , \tag{22}$$

where $x = q_0/|\mathbf{q}|$ and ϕ is the angle between the components of the velocities of the incoming particles transverse to the momentum transfer $\mathbf{q}$. While q_0 is small, the momentum transfer $\mathbf{q}$ can be larger since the maximum angle by which electrons can scatter on the Fermi surface is set by the upper bound in Eq. (19).

The longitudinal and transverse self-energies Π_L and Π_T are in general complex functions of q_0 and $|\mathbf{q}|$. These self-energies can be obtained in the hard dense loop approximation [2]. Since the exchanged photon also has small energy, we will use approximate forms [31] in the nearly static limit $q_0/|\mathbf{q}| \ll 1$:

$$\Pi_L = m_D^2 \quad \text{and} \quad \Pi_T = i\frac{\pi}{4}\frac{q_0}{|\mathbf{q}|}m_D^2 \quad . \tag{23}$$

For degenerate unpaired quark matter

$$m_D^2 = (\sum z_i^2 e^2)\ \mu_q^2\,, \tag{24}$$

where $z_i = +2/3$ or $-1/3$ is the charge of the unpaired quark species i.

In the 2SC phase, up and down quarks of one color are unpaired. Strange quarks can be unpaired or form a spin one condensate which breaks rotational invariance. For the paired quarks in the 2SC phase, photon-gluon mixing can occur. The residual $U(1)$ symmetry is a combination of the electric charge Q and the $SU(3)$ hypercharge T_8. The Debye mass associated with the photon is given by [32]

$$m_D^2 = \frac{2e^2\mu_q^2}{3\pi^2}\,, \tag{25}$$

where μ_q is the quark chemical potential, of order hundreds of MeV. For degenerate electrons,

$$m_D^2 = e^2\mu_e^2/3\,. \tag{26}$$

In what follows, we denote the phase dependent screening mass by m_D, noting that its magnitude is generally larger than m_e. Contributions to the emissivity from screened electric effects will turn out to be much smaller than those from unscreened magnetostatic modes.

It is easier to evaluate $d\sigma_{el}$, a Lorentz invariant quantity, in the CM frame, and later transform to laboratory co-ordinates for the final phase space integrations. In the CM frame, elastic scattering between identical particles implies that $q_0 = 0$ and $\cos\phi = -1$. If the scattering angle θ_{lab} is small, so is the scattering angle θ_{CM} in the CM frame since $\theta_{CM} = 2\theta_{lab}$ for identical particles. Moreover, $q^2 = -\mathbf{q}^2 = -E_1E_3\theta_{CM}^2$. The elastic differential cross-section then simplifies to

$$\begin{aligned} d\sigma_{el} = \frac{1}{2E_1}\frac{1}{2E_2}\int \frac{d^3p_3}{(2\pi)^3 2E_3}\frac{d^3p_4}{(2\pi)^3 2E_4} 16e^4E_1^2E_2^2 \left|\frac{1}{E_1E_3{\theta_{CM}}^2 + m_D^2} + \frac{1}{E_1E_3{\theta_{CM}}^2}\right|^2 \\ \times(2\pi)^3\delta^3(\mathbf{P_1}+\mathbf{P_2}-\mathbf{P_3}-\mathbf{P_4})2\pi\delta(E_1+E_2-E_3-E_4)\tilde{n}_F(E_3)\tilde{n}_F(E_4) \quad . \end{aligned} \tag{27}$$

Denoting the total CM energy as $E_1+E_2 = 2\mathcal{E}$ and using the momentum conserving delta-function to perform the d^3p_4 integration, we find

$$d\sigma_{el} = 2\alpha^2\mathcal{E}^2\int\frac{d^3p_3}{E_3^2}\left|\frac{1}{E_1E_3{\theta_{CM}}^2 + m_D^2} + \frac{1}{E_1E_3{\theta_{CM}}^2}\right|^2 \delta(\mathcal{E}-E_3)(\tilde{n}_F(E_3))^2 \quad , \tag{28}$$

where $\alpha = e^2/4\pi$ is the fine structure constant. Since the main contribution comes from the vicinity of the Fermi surface, we can change variables as $d^3p_3 \approx E_3^2 dE_3 d\Omega_{p_3}$ (the mass of the electron can be safely ignored here). The delta function facilitates the integration over $d|\mathbf{p_3}|$ with the result

$$d\sigma_{el} = \frac{2\alpha^2}{\mathcal{E}^2}(\tilde{n}_F(\mathcal{E}))^2\int d\Omega_{p_3}\left(\frac{1}{\theta_{CM}^2+a^2}+\frac{1}{\theta_{CM}^2}\right)^2; \quad a = m_D/\mathcal{E} \quad . \tag{29}$$

Without loss of generality, we can take $\mathbf{P_1}$ and $\mathbf{P_2}$ to be along $\hat{\mathbf{z}}$ and $-\hat{\mathbf{z}}$, respectively, so that $d\Omega_{p_3} = d\Omega_{CM}$. It can be checked at this stage that we recover the vacuum result for Møller scattering. If the blocking factors from the above expression are set to unity, and $a = 0$, we find

[2] We are ignoring the smaller contribution from finite temperature effects (hard thermal loops).

$$\frac{d\sigma_{el}}{d\Omega_{CM}} = \frac{4\alpha^2}{\mathcal{E}^2\theta_{CM}^4} \quad , \tag{30}$$

which is the most singular part of the Møller cross-section in the ultra-relativistic limit. (In making the comparison, a symmetrizing factor of 1/2 has to be reinserted, because particles in the initial state are indistinguishable). Returning to the in-medium expression Eq. (29), we note that the integral over $d\theta_{CM}$ should also include the θ_{CM}-dependence from $F(\xi)$. Integrating ϕ from 0 to 2π, and θ_{CM} from θ_{min} to θ_{max} as prescribed by Eq. (19), we obtain

$$d\sigma'_{el} = \frac{4\pi\alpha^2}{\mathcal{E}^2}(\tilde{n}_F(\mathcal{E}))^2\left[\ln\left(\frac{\theta_{max}}{\theta_{min}}\right) + \frac{3}{2}\ln\left(\frac{\theta_{max}^2+a^2}{\theta_{min}^2+a^2}\right) + \frac{a^2}{2}\left(\frac{1}{\theta_{max}^2+a^2} - \frac{1}{\theta_{min}^2+a^2}\right)\right] \quad . \tag{31}$$

The prime on $d\sigma_{el}$ is to remind us that the angle-dependent part from photon emission must also be included in performing the angular integral in the elastic cross-section. Next, the $d\omega_k$ integral in Eq. (14) is to be performed. The lower limit on ω_k is $\omega_{min} = \omega_p$, while the upper limit is $\omega_{max} \approx \sqrt{\omega_p^2 + m_e^2}$. The upper limit is set by noting that for small angles, we can write $|\mathbf{k}|_{max} \approx E\theta_{max} \approx E(m_e/E) = m_e$. Although photons of energy $\omega_k > \omega_{max}$ are also emitted, their contribution, which cannot be included consistently within our approximations, is expected to be small in the degenerate limit.

The integral over ω_k can be rewritten as

$$\int d\omega_k\, \omega_k\left(\frac{d\sigma}{d\omega_k}\right) = \frac{32\alpha^3}{5\mathcal{E}^2}(\tilde{n}_F(\mathcal{E}))^2\int_{\omega_{min}}^{\omega_{max}} d\omega_k n^3\Big\{I_1 + I_2 + I_3\Big\} \quad , \tag{32}$$

where

$$I_1 = \ln\left(\frac{E^2}{m_e\omega_k}\right) \quad , \tag{33}$$

$$I_2 = \frac{3}{2}\left[\ln\left(\frac{m_e^2+m_D^2}{E^2}\right) - \ln\left(\left(\frac{m_e^2\omega_k}{E^3}\right)^2 + \frac{m_D^2}{E^2}\right)\right] \quad , \tag{34}$$

$$I_3 = \frac{m_D^2}{2(m_e^2+m_D^2)} - \frac{m_D^2E^4}{2m_e^4}\frac{1}{(\omega_k^2 + (\frac{m_DE^2}{m_e^2})^2)} \quad . \tag{35}$$

The Debye mass $m_D \gg m_e$, which allows us to drop contributions from I_2 and I_3, and retain the largest contribution from I_1. This contribution is easy to evaluate, since ω_p is a slowly varying function of the distance z for temperatures less than 1 MeV [21]. The logarithmic factor in Eq. (33) is only weakly dependent on ω_k as compared to the square root prefactor and can therefore be pulled out of the integral with only a slight underestimation of the integral. This leads to the expression

$$\int \omega_k d\sigma = \frac{64\alpha^3 m_e}{5\mathcal{E}^2}(\tilde{n}_F(\mathcal{E}))^2\ln\left(\frac{E}{m_e}\right)\left\{1 + \frac{1}{2}\frac{\omega_p^2}{\omega_p^2+m_e^2} - \frac{3}{2}\tan^{-1}\left(\frac{m_e}{\omega_p}\right)\right\} \quad . \tag{36}$$

Inserting this result in Eq. (14), the emissivity becomes

$$Q = \frac{64\alpha^3 m_e}{5\hbar}\int\frac{d^3p_1}{(2\pi)^3}\frac{d^3p_2}{(2\pi)^3}n_F(\omega_{p_1})n_F(\omega_{p_2})\frac{\tilde{n}_F(\mathcal{E})^2}{\mathcal{E}^2}\ln\left(\frac{E}{m_e}\right)\left\{1 + \frac{1}{2}\frac{\omega_p^2}{\omega_p^2+m_e^2} - \frac{3\omega_p}{2m_e}\tan^{-1}\left(\frac{m_e}{\omega_p}\right)\right\} \quad . \tag{37}$$

We note that electric effects are not very important for the conditions of interest here, since they are strongly supressed because $(m_e/m_D)^2 \ll 1$. We have therefore dropped contributions of $\mathcal{O}\Big(m_e^2/m_D^2\Big)$. As we have focused on soft exchanges, the magnetic damping for such modes vanishes; consequently they provide the largest contribution to the integral.

For strongly degenerate electrons, further reduction of Eq. (37) is afforded by the nearly step function character of the Fermi functions. We can approximate $E \approx \mu_e$, so that the logarithmic factor is now a constant and can be pulled out of the integral. The variable $\mathcal{E}$ can be converted to laboratory coordinates using the relation

$$\mathcal{E} = \left\{\frac{|\mathbf{P_1}||\mathbf{P_2}|}{2}(1-\cos\theta_{12}) + \frac{m_e^2}{4}\left(2 + \frac{|\mathbf{P_1}|}{|\mathbf{P_2}|} + \frac{|\mathbf{P_2}|}{|\mathbf{P_1}|}\right)\right\}^{1/2} \quad , \tag{38}$$

$$\cos\theta_{12} = \cos\theta_1\cos\theta_2 + \sin\theta_1\sin\theta_2\cos(\phi_1-\phi_2) \quad .$$

We can further set $|\mathbf{P_1}|, |\mathbf{P_2}| \approx p_{F_e}$, the electron Fermi momentum so that $\tilde{n}_F(\mathcal{E})$ depends only on the angular variables θ_1 and θ_2. The integral over the momenta can be evaluated approximately in the degenerate limit:

$$\mathcal{N}(T,\mu_e)=\int dp\frac{p^2}{\mathrm{e}^{(\sqrt{p^2+m_e^2}-\mu_e)/T}+1}\longrightarrow\frac{\mu_e^3}{3}\left[1+\left(\frac{\pi T}{\mu_e}\right)^2+\mathcal{O}\left(\frac{m_e^4T^4}{\mu_e^8}\right)+...\right]\quad . \tag{39}$$

Terms involving the electron mass can be dropped because they appear only beyond second order in the above expansion. More details on the evaluation of the angular integral are given in Appendix A. Here, we quote the final result for the emissivity in two relevant limits:

$$Q=\frac{64\alpha^3m_e\mathcal{F}(\omega_p)(\mathcal{N}(T,\mu_e))^2}{5\hbar(2\pi)^6}\ln\left(\frac{\mu_e}{m_e}\right)\mathcal{I}(T,\mu_e) \tag{40}$$

$$\mathcal{F}(\omega_p)=\left\{1+\frac{1}{2}\frac{\omega_p^2}{\omega_p^2+m_e^2}-\frac{3\omega_p}{2m_e}\tan^{-1}\left(\frac{m_e}{\omega_p}\right)\right\}$$

$$\mathcal{I}(T,\mu_e)=8\pi^2\times\left\{\begin{array}{c}\frac{4T}{\mu_e^3}\left(\ln 2-\frac{1}{2}\right);\quad \frac{m_e^2}{2\mu_e}\leq T\ll\mu_e\\ \frac{2}{\mu_e^2}\mathrm{e}^{-m_e^2/2\mu_eT};\quad T\ll\frac{m_e^2}{2\mu_e}\end{array}\right\}.$$

Note that $\mathcal{F}(\omega_p)\to 1$ for $\omega_p\ll m_e$ and $\mathcal{F}(\omega_p)\to(m_e/\omega_p)^4/5$ for $\omega_p\gg m_e$.

Equation (40) provides the photon emissivity to logarithmic accuracy. A better estimate can be obtained by a numerical integration of Eq. (37) which can be reduced to a five-dimensional integral by choosing, for example, the azimuthal angle $\phi_2=0$. The limits on ϕ_1 then run from 0 to 2π, and θ_1 and θ_2 each range from 0 to π. In the degenerate limit, the Fermi functions cause the integrand in Eq. (37) to be strongly peaked for radial momenta $p_1\approx p_2\approx\mu_e$. In this case, it is advantageous to use an adaptive Monte-carlo method such as VEGAS [33], which is based on stratified importance sampling. We can restrict the range of integration for the radial momenta from $\mu_e-\delta$ to $\mu_e+\delta$, where $\delta\ll\mu_e$ is chosen to be a suitable multiple of the temperature. This procedure provides an accuracy of better than a few percent.

If the temperature becomes comparable to μ_e, electrons cannot be considered as degenerate and our approximations would not be valid. In our numerical calculations therefore, temperatures are chosen to be much smaller than μ_e. Within the temperature limits that set the validity of our expressions, one can compare the photon emissivity from e^-e^- bremsstrahlung to that of e^+e^- pairs [34]. Such comparisons are presented below.

B. Comparison with Other Processes

For purposes of comparison and easy estimation, it is useful to express all fluxes in terms of typical temperatures and chemical potentials. We will employ T_9 to denote the temperature in units of 10^9K, and μ_{10} to represent the electron chemical potential in units of 10 MeV. The result for the bremsstrahlung radiation flux from Eq. (40) can then be recast as

$$F=\int_{z=0}^{z=z_0}dz\;Q\,;\quad Q=1.14\times10^{42}\left\{1+\frac{0.15\mu_{10}^2}{0.3\mu_{10}^2+0.26}-1.61\mu_{10}\tan^{-1}\left(\frac{0.92}{\mu_{10}}\right)\right\}\mu_{10}^4\left[1+\frac{\pi^2}{256}\left(\frac{T_9}{\mu_{10}}\right)^2\right]^2 \tag{41}$$

$$\times\ln(19.6\mu_{10})\times\left\{\begin{array}{c}\frac{0.034T_9}{\mu_{10}}\left(\ln2-0.5\right);\ \frac{0.15}{\mu_{10}^2}\leq\frac{T_9}{\mu_{10}}\ll116\\ 0.02\ \mathrm{e}^{-0.15/T_9\mu_{10}};\ T_9/\mu_{10}\ll0.15\end{array}\right\}\mathrm{erg\ cm^{-3}s^{-1}}.$$

where z_0 is the thickness of the electrosphere. The plasma frequency of a highly degenerate electron plasma depends linearly on the chemical potential (see Eq. (6)) and has been rescaled accordingly ($\omega_p(z)=0.55\mu_{10}(z)$ MeV). Excepting the outermost regions of the electrosphere, we can safely assume the electrons to be degenerate for all chemical potentials and temperatures considered in this work. The flux (similarly re-expressed) from the pair creation process is [34]

$$F_\pm=\int_{z=0}^{z=z_0}dz\;Q_\pm\;;\quad Q_\pm=4.52\times10^{42}\{0.51+0.0862T_9\}\mu_{10}T_9^3\left[1+\frac{\pi^2}{256}\left(\frac{T_9}{\mu_{10}}\right)^2\right]^2 \tag{42}$$

$$\times\exp\left(-\frac{11.83}{T_9}\right)J\left(\frac{11.6\mu_{10}}{T_9}\right)\ \mathrm{erg\ cm^{-3}s^{-1}}\quad ,$$

where

$$J(x)=\frac{1}{3}\frac{x^3\ln(1+2/x)}{(1+0.074x)^3}+\frac{\pi^5}{6}\frac{x^4}{(13.9+x)^4}\quad . \tag{43}$$

The blackbody flux is given by the Stefan-Boltzmann law:

$$F_{BB} = 5.67 \times 10^{31} T_9^4 \text{ erg cm}^{-2}\text{s}^{-1} . \tag{44}$$

For illustration, we choose $T_9 = 1$, an electrosphere thickness $z_0 = 1000$ fm and $\mu_{10}(0) = 1$. With the electron density profile given by Eq. (4), we find

$$\begin{aligned} F &= 9.06 \times 10^{28} \text{ erg cm}^{-2} \text{ s}^{-1} \\ F_{\pm} &= 1.45 \times 10^{28} \text{ erg cm}^{-2} \text{ s}^{-1} \\ F_{BB} &= 5.67 \times 10^{31} \text{ erg cm}^{-2} \text{ s}^{-1} \quad . \end{aligned} \tag{45}$$

These numbers demonstrate that the bremsstrahlung radiation flux from e^-e^- scattering in the electron layer dominates over that from pair creation.

In Fig. 2, we compare the flux from the bremsstrahlung process to that from the pair creation process, both scaled to the blackbody limit. For simplicity and for the sake of comparison with the analytical result Eq. (40), we assume a uniform chemical potential. In this case, the integral over z gives simply z_0, the thickness of the electrosphere. To be consistent, we take the thickness to be $z_0 = 100$ fm for which the chemical potential changes only by about 20% . The analytical estimate in Eq. (40) agrees well with results from numerical integrations of Eq. (37). For $T_9 \leq 2$, the flux from the bremsstrahlung process is more than that from the pair creation process (it may even dominate at somewhat higher temperatures once the contribution from higher energy photons is included.) whereas for temperatures $T_9 > 2$, the flux from the pair creation process exceeds that from bremsstrahlung. (This conclusion is not significantly modified upon the inclusion of LPM effects, as we will see.) Thus, for electron plasmas below a temperature of ~ 0.1 MeV, bremsstrahlung radiation is an important channel for photon cooling of bare quark stars. Its dependence on the third power of the electron chemical potential (or linear in electron density) distinguishes it from other processes.

With increasing electron degeneracy (value of μ_e/T) or electrosphere thickness z_0, the flux from bremsstrahlung rapidly increases until it starts to become comparable to the blackbody limit. At this stage, the inverse process, photon absorption on electrons and rescattering (Comptonization) becomes important and the opacity of the layer increases. Detailed balance then implies that the blackbody limit is saturated, and the electrosphere radiates like a blackbody. The inverse processes have not been taken into account in the curves of Fig. 2, hence they appear to exceed the blackbody limit for some temperatures. However, there exists a window, $0.1 < T_9 < 1$, in which the inverse processes can be neglected and in which the bremsstrahlung flux exceeds that from pair creation.

C. Spectral Features and Typical Energies

The spectrum of low energy bremsstrahlung photons can be read off from Eq. (32). Explicitly,

$$\omega_k \left(\frac{d\sigma}{d\omega_k} \right) \propto \left(1 - \frac{\omega_p^2}{\omega_k^2} \right)^{3/2} \ln\left(\frac{\mu_e^2}{m_e \omega_k} \right) \quad , \tag{46}$$

where in the term involving the logarithm the electron energy E has been replaced by μ_e. In the quasiclassical approximation employed here, support for this spectrum exists only between $\omega_{min} = \omega_p$ and $\omega_{max} = (\omega_p^2 + m_e^2)^{1/2}$. One must go beyond the quasiclassical approximation in order to obtain the spectrum for $\omega > \omega_{max}$. In vacuum, the low energy bremsstrahlung spectrum for frequencies $\mu_e - \omega_k \gg m_e$ reads [27]

$$\omega_k \left(\frac{d\sigma}{d\omega_k} \right) \propto x \left(1 - \frac{\omega_p^2}{\omega_k^2} \right)^{1/2} \left(x + \frac{1}{x} - \frac{2}{3} \right) \left[\ln\left(\frac{2x\mu_e^2}{m_e \omega_k} \right) - \frac{1}{2} \right]; \quad x = 1 - \frac{\omega_k}{\mu_e} . \tag{47}$$

For typical values of μ_e encountered across the electrosphere, Fig. 3 shows the role of medium effects by comparing the low energy spectrum with the low energy spectrum neglecting all medium effects (except the plasma cutoff).

Although photons are emitted from thermal electrons, the non-thermal character of the bremsstrahlung radiation is evident from this figure. While this is a natural feature of any spectrum calculated with a low-energy cut-off, the large mean free path of photons in the electrosphere, and medium modifications reinforce the same physical conclusion even if the entire range of frequencies is covered. The extra factor of n^2 induced by bremsstrahlung in the medium produces a harder spectrum than in vacuum, while the total flux is smaller. The spectrum of high energy photons is expected to fall off steeply due to the large electron degeneracy. However, as mentioned previously, this feature cannot be calculated within the quasiclassical approximation made here.

We turn now to estimate the characteristic energies of the emitted photons, and to contrast them with those characteristic of thermal blackbody radiation. In order to perform these tasks, we examine the quantities

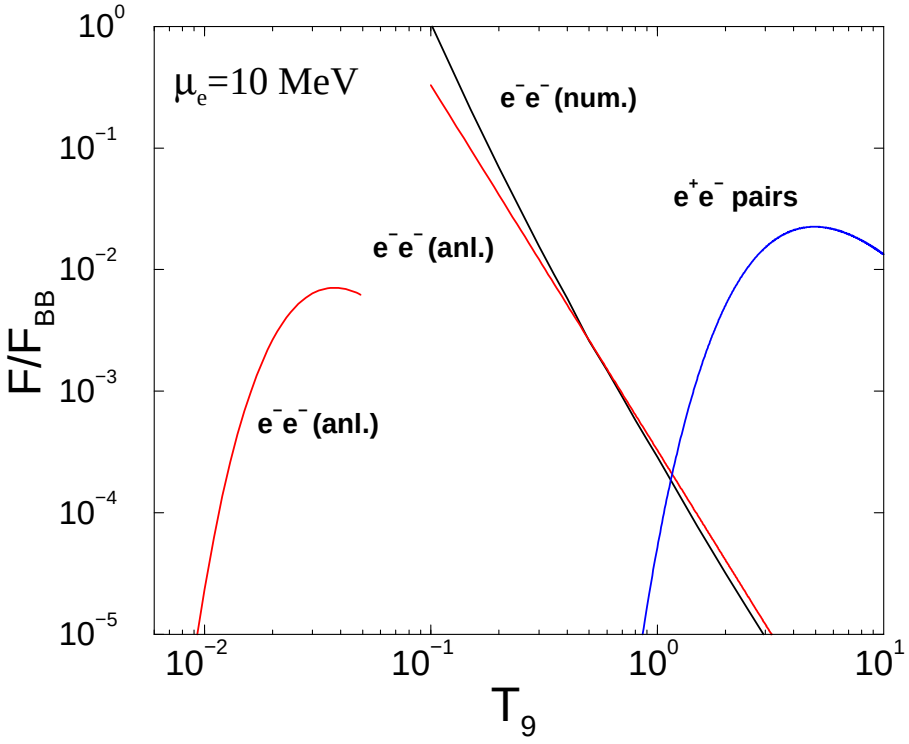

FIG. 2. Photon fluxes from the bremsstrahlung and pair creation processes scaled to the blackbody limit as a function of temperature in units of 10^9K (T_9). The curve marked (num.) shows results of numerical integrations of Eq. (37) which is to be compared with the results of the analytical expressions (anl.) from Eq. (40) for low and high temperatures. The (uniform) electron chemical potential is $\mu_e = 10$ MeV with $z_0 = 100$ fm.

$$\begin{pmatrix} \Gamma \\ Q \\ Q^2 \end{pmatrix} = \frac{1}{\hbar}\int \frac{d^3p_1}{(2\pi)^3}\frac{d^3p_2}{(2\pi)^3} n_F(\omega_{p_1}) n_F(\omega_{p_2}) \int d\omega_k \begin{pmatrix} 1 \\ \omega_k \\ {\omega_k}^2 \end{pmatrix} \left(\frac{d\sigma}{d\omega_k}\right), \tag{48}$$

where Γ is the number of bremsstrahlung reactions per unit volume per unit time (the rate), Q is the energy loss in photons per unit volume per unit time (the emissivity), and Q^2 is the squared energy loss per unit volume per unit time. Good measures of the average photon energy and the average squared photon energy are provided by the ratios

$$\langle\omega\rangle = Q/\Gamma \qquad \text{and} \qquad \langle\omega^2\rangle = Q^2/\Gamma\,. \tag{49}$$

It is also instructive to examine the dimensionless ratio

$$R = \langle\omega^2\rangle/\langle\omega\rangle^2\,, \tag{50}$$

which can be used to gauge the gross spectral features of the energy spectrum. The quantity R takes into account the full effects of the transition amplitudes and 4-momentum conservation.

The calculations of Γ (this is finite because of the finite plasma frequency) and Q^2 for the bremsstrahlung process can be performed following the procedure adopted for the calculation of Q in Sec. III A. The results are

$$\Gamma = Q\frac{\mathcal{H}(\omega_p)}{\mathcal{F}(\omega_p)}; \quad \mathcal{H} = \left[\frac{1}{m_e}\ln\left(\frac{m_e+\sqrt{\omega_p^2+m_e^2}}{\omega_p}\right) - \frac{3\omega_p^2+4m_e^2}{3(\omega_p^2+m_e^2)^{3/2}}\right] \tag{51}$$

$$Q^2 = Q\frac{\mathcal{G}(\omega_p)}{\mathcal{F}(\omega_p)}; \quad \mathcal{G} = \left[\frac{3\omega_p^2+m_e^2}{2\sqrt{\omega_p^2+m_e^2}} - \frac{3\omega_p^2}{2m_e}\ln\left(\frac{m_e+\sqrt{\omega_p^2+m_e^2}}{\omega_p}\right)\right], \tag{52}$$

where the quantities Q and $\mathcal{F}$ are given in Eq. (40). The average photon energy is therefore

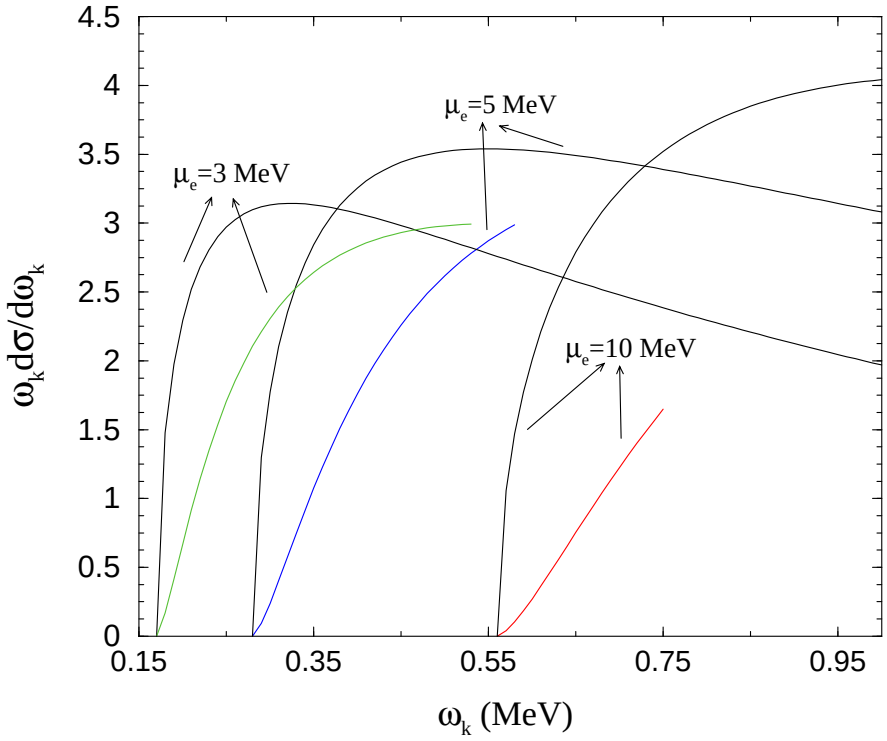

FIG. 3. The energy spectrum of bremsstrahlung photons at the indicated values of the electron chemical potential μ_e. The full curves are the spectrum from Eq. (32), while the truncated curves correspond to Eq. (47) for the low energy spectrum in vacuum valid for frequencies satisfying the condition $\mu_e - \omega_k \gg m_e$.

$$\langle\omega\rangle = \frac{\mathcal{F}}{\mathcal{H}} \to \begin{cases} \omega_p & \text{for } \omega_p \gg m_e \\ m_e/\ln(2m_e/\omega_p) & \text{for } \omega_p \ll m_e \end{cases} . \tag{53}$$

In Fig. 4, we show the mean energy of photons versus distance in the electrosphere for $\mu_e(0) = 10$ MeV and $T = 1$ MeV. The solid curve shows the result obtained by using the analytical expression for $\langle\omega\rangle = \mathcal{F}/\mathcal{H}$. Results obtained by numerical integrations of Eq. (37) and its counterpart for Γ are shown by the dashed curve. It is clear that the analytical results give a fairly accurate representation of the numerical results for values of ω_p sampled across the electrosphere (see Fig. 1). The mean energy of photons varies from 0.4 MeV to 0.7 MeV, depending on the depth from which the photons are emitted. On average, this is larger than the mean energy of 0.5 MeV from the annihilation of e^+e^- pairs. This is also very different from the spectrum of photons from a normal cooling neutron star with $0.1 < E/\text{keV} < 2.5$.

The ratio R is given by

$$R = \frac{\mathcal{G}\mathcal{H}}{\mathcal{F}^2} \to \begin{cases} 1 & \text{for } \omega_p \gg m_e \\ \frac{1}{2}\ln\left(\frac{2m_e}{\omega_p}\right) & \text{for } \omega_p \ll m_e \end{cases} \tag{54}$$

In order to highlight the differences between the bremsstrahlung and blackbody radiation, the quantities $\langle\omega\rangle$ and R can be contrasted with the ideal gas benchmark quantities.

$$R_{id} = \frac{\langle\omega^2\rangle_{id}}{\langle\omega\rangle^2_{id}} \qquad \text{with} \qquad \begin{pmatrix} \langle\omega\rangle_{id} \\ \langle\omega^2\rangle_{id} \end{pmatrix} = \frac{\displaystyle\int_0^\infty dk\ k^2 \begin{pmatrix} \omega \\ \omega^2 \end{pmatrix} F_\gamma(\omega)}{\displaystyle\int_0^\infty dk\, k^2 F_\gamma(\omega)} , \tag{55}$$

where F_γ is the equilibrium Bose-Einstein distribution function characterizing in-medium photons with mass ω_p and zero chemical potential. Explicitly,

$$\langle\omega\rangle_{id} \to \begin{cases} \omega_p + \frac{3}{2}T & \text{for } \omega_p \gg T \\ \dfrac{\Gamma(4)\zeta(4)}{\Gamma(3)\zeta(3)}\ T \simeq 2.7\ T & \text{for } \omega_p \ll T \end{cases} \tag{56}$$

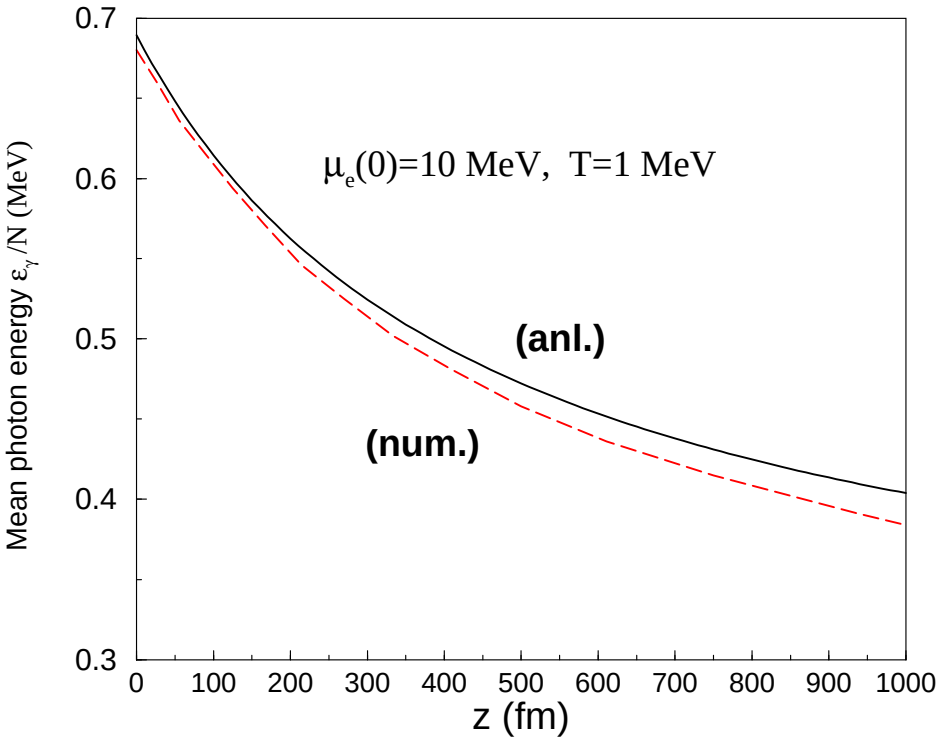

FIG. 4. The mean photon energy as a function of distance in the electrosphere. The solid curve shows results from the analytical expression in Eq. (52), while the dashed curve is obtained by numerical integrations of Q in Eq. (37) and its counterpart Γ. Numerical values of the electron chemical potential μ_e and temperature T are as shown in the inset.

$$\langle\omega^2\rangle_{id} \rightarrow \begin{cases} \omega_p^2 + 3mT & \text{for } \omega_p \gg T \\ \dfrac{\Gamma(5)\zeta(5)}{\Gamma(3)\zeta(3)}\, T^2 \simeq 10.35\, T^2 & \text{for } \omega_p \ll T \end{cases} \tag{57}$$

These results imply that [35]

$$R_{id} \rightarrow \begin{cases} 1 & \text{for } \omega_p \gg T \\ 1.42 & \text{for } \omega_p \ll T \end{cases} \tag{58}$$

The behaviors of R versus ω_p/m_e and R_{id} versus ω_p/T are compared in Fig. 5, which highlights the non-thermal nature of the bremsstrahlung radiation emitted from degenerate electrons. In light of the limited frequency support for bremsstrahlung, a more rigorous quantum calculation is called for to characterize the spectrum more accurately.

D. Inclusion of the Landau-Pomeranchuk-Migdal Effect

As noted in Sec. II, multiple scattering of electrons within the formation time of the radiated photon can lead to the so-called LPM suppression of bremsstrahlung. We had omitted a detailed consideration of this effect in order to isolate the T and μ_e-dependences of the emissivity in the absence of the LPM effect. Since an analytical estimate including LPM suppression is cumbersome, we have performed a numerical integration of Eq. (37) utilizing the approximate suppression factor $S_{LPM}(k)$ from Eq. (12).

In Fig. 6, the effects of the LPM effect are assessed. The LPM effect reduces the simple analytical estimate in Eq. (40) by a significant amount. Specifically, for $\mu_{10} = 1$, the reduction factor (relative to the emissivity without the LPM effect) is ~ 60, while for $\mu_{10} = 2$, the reduction factor is ~ 350. The temperature range is $0.1 < T_9 < 10$. The suppression is stronger at higher densities (compare the left and right panels), since the density of scatterers controls the LPM effect. The suppression factor for $\mu_{10} = 0.5$ (not shown in the figure) is approximately a factor of 10.

The mean photon energy Q/Γ does not change much from the analytical estimate upon the inclusion of the LPM suppression factor. This is because both the rate and the energy loss are affected similarly and therefore the LPM effect nearly cancels in the

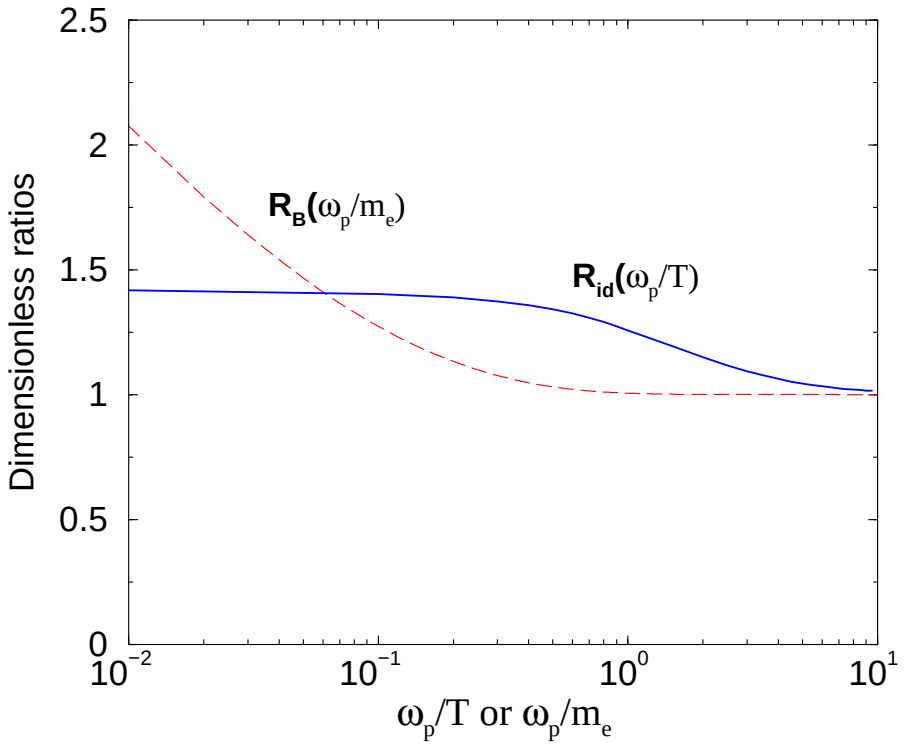

FIG. 5. A comparison of the ratio R in Eq. (54) for bremsstrahlung photons and R_{id} in Eq. (55) for thermal photons with in-medium photon mass ω_p.

ratio. For the same reason, the LPM suppression does not significantly change the shape of the spectra discussed in the previous section. The spectra are controlled primarily by the ratio of plasma frequency to electron mass.

Equilibrium radiation from quark matter and bremsstrahlung radiation from quark-quark collisions in the surface layers also produce photons. In Ref. [36], luminosities from these processes were compared to the blackbody luminosity; it was found that for $T \leq 2 \times 10^{10}$ K (i.e., $T_9 < 20$), the equilibrium radiation is negligible. For these temperatures, the non-equilibrium radiation from quark-quark Bremstrahlung dominates, although it is still 4 orders of magnitude less than the blackbody luminosity (even this may be an overestimate according to Ref. [34]). Accounting for the multiple scattering (LPM effect) of quarks and absorption by the electron layer leads to the conclusion that an additional suppression by 2 orders of magnitude is likely [37], so that overall, the photon emissivity from quark matter is about 6 orders of magnitude smaller than the blackbody emissivity. The dominant contribution thus comes from e^+e^- pair production via the Schwinger mechanism in the presence of strong electric fields or the e^-e^- bremsstrahlung process in the thin electron layer. The relative importance of these two processes depends sensitively on the temperature.

In the range $T \leq 10^9$K, bremsstrahlung is the dominant emission process, since the emissivity from the pair creation process is vanishingly small. The analytical treatment of the bremsstrahlung process performed in this work provides a good approximation to the numerical results in this range of temperatures. At low temperatures ($T \leq 10^7$ K), the bremsstrahlung rate is exponentially small as seen from Eq. (40). For temperatures in the range $T \sim 10^8$K, the inverse process of photon absorption also becomes important as the rate approaches the blackbody limit. The main conclusion is that for temperatures $T < 10^9$K, the bremsstrahlung process is likely to be the dominant photon emission source, even in the presence of LPM effects, when compared to the annihilation of e^+e^- pairs.

IV. CONCLUSIONS AND OUTLOOK

We have calculated the photon emissivity from the $e^-e^- \to e^-e^-\gamma$ bremsstrahlung process occurring in the electrosphere of a bare strange quark star. For degenerate electrons and for low energy photons, unscreened magnetic interactions provide the largest contribution to the emissivity, while the contribution from screened electric interactions is comparatively negligible. For temperatures in the range 10^8K$< T < 10^9$K, the emissivity from the bremsstrahlung process surpasses that of the e^+e^- pair

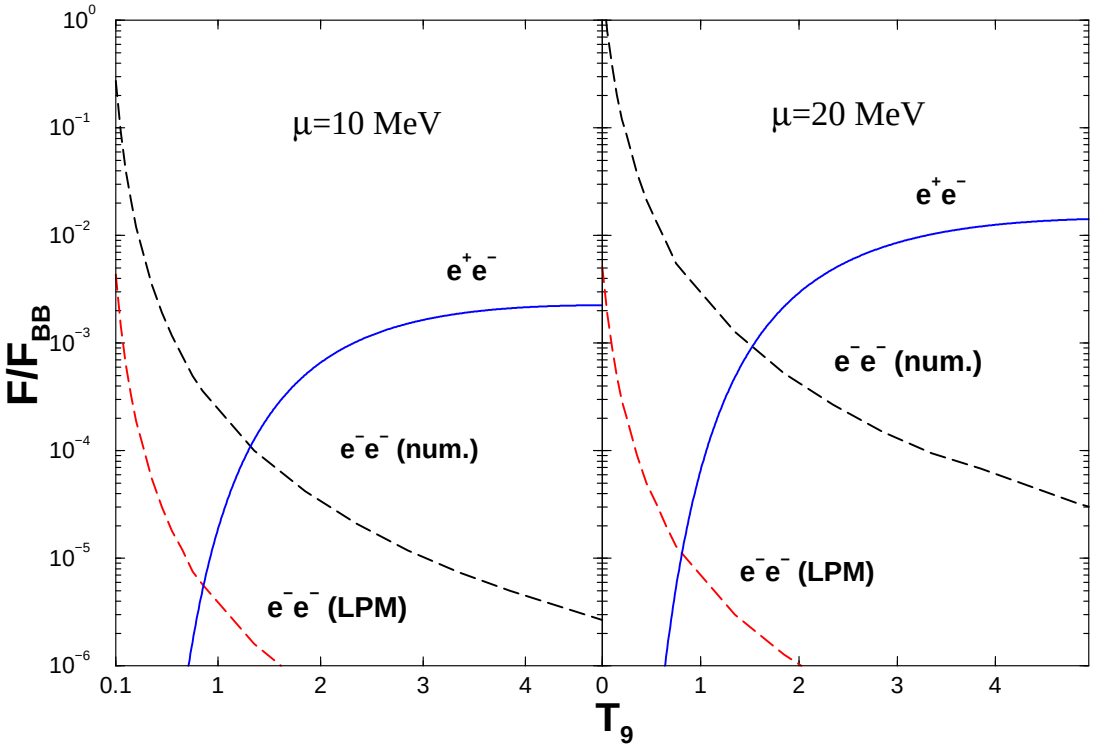

FIG. 6. Photon fluxes from the bremsstrahlung and pair creation processes scaled to the blackbody value as a function of temperature in units of 10^9K (T_9). In the case of the bremsstrahlung process, the upper (lower) curve shows results without (with) the effects of the Landau-Pomeranchuk-Migdal effect. Numerical values of the electron chemical potentials are as indicated.

production process occurring in the presence of a strong electric field in the electrosphere. Within the soft photon approximation, the mean energy of the bremsstrahlung photons escaping the electrosphere is ~ 0.5 MeV. This estimate may be slightly altered if the entire spectrum is sampled. Under strongly degenerate conditions, the contribution of high energy photons to the emissivity is expected to be small in comparison to that from low energy photons.

Photons from the bremsstrahlung process are non-thermal for sufficiently thin electrospheres and moderate electron chemical potentials, because such photons do not undergo sufficient number of scatterings in the electrosphere. Inclusion of the Landau-Pomeranchuk-Migdal effect, which arises due to multiple scatterings of the emitting electron, reveals that even in the presence of a large suppression from this effect the bremsstrahlung process emerges as the dominant source of radiation from the star's surface for temperatures in the range $10^8\text{K} < T < 10^9\text{K}$. We may regard the LPM-inclusive bremstrahlung rates as a conservative estimate, since we have approximated photon exchange by a static Coulomb field. If retardation effects were included, the suppression will be smaller leading to somwewhat higher rates. Both the "bare" and LPM-corrected rates take into account the dielectric suppression effect of the electrosphere. The consequence is that the LPM suppression is two orders of magnitude less than that in the case the photon is emitted into vacuum. There is an additional mitigating effect of about 15% on the LPM suppression due to the strong external electric field, which can bend the electron trajectory causing the formation time of the emitted photon wave packet to decrease. This implies that the emission angles can be increased beyond $\theta_{max} = m_e/E$. However, this only changes the emissivity by a pre-factor $\sim 4/3$, and to logarithmic accuracy our principal results are valid even in the presence of strong electric fields. In view of this, our LPM-corrected rates should be treated as a lower bound.

An intriguing result of our calculations is that for $T \leq 10^{-3}\ \mu_e(0)$, bremsstrahlung emission becomes comparable to blackbody emission. This indicates that bremstrahlung absorption has to be taken into account in estimating the optical thickness of the electrosphere (see the discussion following Eq. (5)). This will lead to better estimates of the emissivity applicable in the temperature window excluded by Eq. (42). The remaining task is to perform calculations of the thermal evolution of strange quark matter stars including the non-thermal bremsstrahlung and thermal pair annihilation processes in order to provide baseline calculations of the surface luminosity versus age. Results of such calculations will be reported separately.

ACKNOWLEDGEMENTS

We thank Vladimir Usov for urging us to investigate the bremsstrahlung process in degenerate matter, and Guy Moore for an observation concerning the LPM effect. P.J. and C.G. are supported in part by the Natural Sciences and Engineering Research Council of Canada and in part by the Fonds Nature et Technologies of Quebec. The research of M.P. was supported by the U.S. Department of Energy grant DOE/DE-FG02-87ER-40317 and the NSF grant INT-9802680. The work of D.P. is partially supported by grants from UNAM-DGAPA (PAPIIT-IN112502) and Conacyt (36632-E).

APPENDIX A: ANGULAR INTEGRATION

The factor $\mathcal{I}(T,\mu_e)$ in Eq. (40) is evaluated below. Since only the relative angle between θ_1 and θ_2 enters in the integration, and we integrate over all relative orientations, we can choose a direction $\hat{p}_1 = \hat{z}$ to decouple the two integrations. Then,

$$\int d\Omega_1 \int d(\cos\,\theta) d\phi \; \frac{\tilde{n}_F(\mathcal{E})^2}{\mathcal{E}^2} \tag{A1}$$

$$= 8\pi^2 \int_{-1}^{1} dx \left(\frac{1}{1+\mathrm{e}^{(\mu_e - [\frac{p_{F_e}^2}{2}(1-x)+m_e^2]^{1/2})/T}} \right)^2 \frac{1}{\frac{p_{F_e}^2}{2}(1-x)+m_e^2} \,.$$

Since $p_{F_e} \gg m_e$ and T, the dominant contribution comes from the region around $x \approx -1$; elsewhere the integrand is exponentially suppressed. Therefore, we can restrict the range of x from -1 to $-1+\delta$, where δ is small. Defining $\epsilon = (1+x)/2$, we can integrate ϵ from 0 up to a characteristic $\delta \sim 10(T/\mu_e)$ when the exponential suppression becomes effective. This leads to

$$\mathcal{I} \approx \frac{16\pi^2}{p_{F_e}^2} \int_0^{\delta} \frac{d\epsilon}{(1-\epsilon)} \left(\frac{1}{1+\mathrm{e}^{\mu_e \epsilon/2T}} \right)^2 \approx \frac{32\pi^2 T}{\mu_e^3} \left[\ln 2 - \frac{1}{2} \right] . \tag{A2}$$

This result is valid as long as $m_e^2/2\mu_e T \leq 1$ and is accurate up to corrections of higher powers of T/μ_e. Therefore, it is a better approximation for large electron degeneracies. When $m_e^2/2\mu_e T \gg 1$, the blocking factors approach zero due to increasing degeneracy of the Fermi sphere, and we obtain

$$\mathcal{I} = \frac{16\pi^2}{\mu_e^2} \mathrm{e}^{-m_e^2/2\mu_e T} \,. \tag{A3}$$

This result shows that the emissivity is exponentially small at very low temperatures.

[1] D. Page and V. V. Usov, Phys. Rev. Lett. **89**, 131101 (2002).
[2] See, e.g., J. Knodlseder, astro-ph/0207527.
[3] E. Witten, Phys. Rev. **D30**, 272 (1984);
[4] S. Chin and A. K. Kerman, Phys. Rev. Lett **43**, 1292 (1979).
[5] E. Farhi and R. L. Jaffe, Phys. Rev. **D30**, 2379 (1984).
[6] P. Haensel, J. L. Zdunik and R. Schaeffer, Astron. Astrophys. **160**, 121 (1986).
[7] C. Alcock and A. Olinto, Ann. Rev. Nucl. Part. Sci. **38**, 161 (1988).
[8] J. M. Lattimer and M. Prakash, Astrophys. J. **550**, 425 (2001).
[9] M. Alford, Ann. Rev. Nuc. Part. Sci. **51**, 131 (2001).
[10] Manju Prakash, E. Baron and M. Prakash, Phys. Lett. **B243**, 75 (1990).
[11] M. Alford and S. Reddy, Phys. Rev. **D67**, 074024 (2003).
[12] S. E. Thorsett and D. Chakrabarty, Astrophys. J. **512**, 288 (1999).
[13] K. Rajagopal and F. Wilczek, Phys. Rev. Lett. **86**, 3492 (2001).
[14] M. Alford and K. Rajagopal, JHEP **0206** 031 (2002).
[15] A. W. Steiner, S. Reddy and M. Prakash, Phys. Rev. **D66**, 094007 (2002).
[16] C. Vogt, R. Rapp and R. Ouyed, Nucl. Phys. **A**, *in press*; hep-ph/0311342.

[17] C. Alcock, E. Farhi and A. V. Olinto, Astrophysical Journal **310**, 261 (1986).
[18] J. Schwinger, Phys. Rev. **82**, 664 (1951).
[19] V. V. Usov, Phys. Rev. Lett **80**, 230 (1998).
[20] M. Alford, C. Kouvaris and K. Rajagopal, arXiv:hep-ph/0311286.
[21] C. Kettner, F. Weber, M. K. Weigel and N. K. Glendenning, Phys. Rev. **D51**, 1440 (1995).
[22] S. Ratković, S. I. Dutta and M. Prakash, Phys. Rev. **D67**, 123002 (2003).
[23] L. D. Landau, and I. Pomeranchuk, Dokl. Akad. Nauk. Ser. Fiz. **92**, 535 (1953); A. B. Migdal, Dokl. Akad. Nauk. S. S. S. R. **105**, 77 (1955).
[24] P. L. Anthony, R. Becker-Szendy, P. E. Bosted, M. Cavalli-Sforza, L. P. Keller, L. A. Kelley, S. R. Klein, G. Niemi, M. L. Perl, L. S. Rochester, J. L. White: E146 Collaboration, Phys. Rev. **D56**, 1373 (1997).
[25] R. Blanckenbecler and S. D. Drell, Phys. Rev. **D53**, 6265 (1996).
[26] F. E. Low, Phys. Rev. **110**, 974 (1958).
[27] *Quantum Electrodynamics*, V. B. Berestetskii, E. M. Lifshitz and L. P. Pitaevskii, Pergamon Press © 1982.
[28] H. A. Weldon, Phys. Rev. **D26**, 1394 (1982).
[29] H. Heiselberg and C. J. Pethick, Phys. Rev. **D48**, 2916 (1993).
[30] M. E. Peskin, and D. V. Schroeder, *An Introduction to Quantum Field Theory*, Perseus Books Publishing, Reading, Massachusetts, 1995.
[31] J. I. Kapusta, *Finite-Temperature Field Theory*, © Cambridge University Press, 1989.
[32] A. Schmitt, Q. Wang and D. H. Rischke, arXiv: nucl-th/0311006.
[33] W. H. Press, S. A. Teukolsky, W. T. Vetterling, and B. P. Flannery, *Numerical Recipes in C: The Art of Scientific Computing*, 2nd edition, Cambridge University Press (1992).
[34] V.V. Usov, Astrophys. J. **550**, L179 (2001).
[35] J. Pawlowski and M. Prakash, To be published.
[36] T. Chomaj, P. Haensel and W. Slomiński, Nucl. Phys. **B24**, 40 (1991).
[37] K. S. Cheng and T. Harko, Astrophys. J. **596**, 451(2003).